Wake measurements from a hydrokinetic river turbine

M. Guerra[a,*], J. Thomson[a]

[a] *Applied Physics Laboratory, University of Washington, Seattle, WA, United States*

Abstract

During the boreal summer of 2015, a full-scale hydrokinetic turbine was deployed in the Kvichak river (Alaska), delivering electricity to the village of Igiugig. Here, quantification and analysis of the hydrodynamic modifications in the river caused by the turbine are presented. Field observations are used to produce a unique three-dimensional data set of fluid velocities in the vicinity of turbine before and after turbine deployment. Three dynamic regions are distinguished in the wake. There is a bow wake just upstream of the turbine, where velocities decrease and turbulence increases. There is a near wake just downstream of the turbine, where the reduced velocities recover slightly and the elevated turbulence decays rapidly. Finally, there is a far wake well beyond the turbine, where reduced velocities are persistent and turbulence remains elevated. The results are used in a coarse energy budget for the river, including quantifying the total energy dissipated by turbulence in the near wake. This wake dissipation is found to be almost as large as the energy extracted for electricity generation, even when the turbine is not operational.

*Corresponding author

Email addresses: `mguerrap@uw.edu` (M. Guerra), `jthomson@apl.washington.edu` (J. Thomson)

Keywords: Hydrokinetic energy, tidal energy, cross-flow turbine, turbine wake, environmental effects, field measurements

Contents

1. Introduction

Hydrokinetic energy is a predictable energy source available in streams, rivers, and tidal channels with sufficiently fast water velocities. The extraction of hydrokinetic energy for electricity generation requires the installation of hydrokinetic turbines facing the flow field. As the development of hydrokinetic turbines reaches a commercial stage, it is essential for hydrokinetic energy extraction projects to have detailed information about the hydrodynamics of these natural systems, for both turbine design and resource assessment. In addition to ambient conditions, it is indispensable to understand and quantify the environmental impacts caused by these underwater turbines [1, 2, 3]. Specifically, the study of the wake generated by the turbines is essential in the characterization of hydrodynamic effects. Wake analysis reveals changes to the mean flow and mixing around the turbine, as well as effects farther downstream. The wake extent and its features can have an impact in the distribution and efficiency of additional turbines [4, 5, 6], and the combined wake of turbine arrays can even affect the large-scale hydrodynamics of the environment [7, 8].

The wake of an hydrokinetic turbine is generally characterized by: i) a deficit in the mean flow due to the drag produced by the turbine structure and due to energy extraction; ii) a modification in turbulence due to eddies shed by the structure and the turbine blades; and iii) complex interactions between natural and turbine-induced turbulent structures [9, 6, 10, 11].

The idealized wake of a hydrokinetic turbine gradually expands into a cone shape region to conserve momentum [12]. Turbulent mixing occurs in the boundary of the region between the wake and the undisturbed flow field, bringing energy into the wake region, which smooths the velocity deficit. After several turbine length scales downstream the turbine, the wake is supposed to dissipate and the flow returns to its original conditions [12]. Of course, the flow can never fully 'recover' to original conditions, because kinetic energy is being extracted from the system. In some cases, the natural system converts potential energy to kinetic energy such that a pseudo-recovery can occur, but there is still a net energy loss in the extraction and subsequent wake. The variables that are thought to impact the turbine's wake are the rotor thrust, ambient and device induced turbulence, proximity to boundaries (bed or free surface), and the vertical and horizontal velocity profiles [12].

Much of the research on hydrokinetic turbine wakes has been carried out numerically [13, 14, 15, 16] and at the laboratory scale under simplified and controlled conditions [17, 5, 18, 19, 16, 20]. These studies differ mainly in the type and number of turbines, and in how detailed the turbine and the energy extraction are represented [21]. At the field scale, towing experiments of a vertical cross-flow turbine have been conducted in an unconfined environment in Polagye et al. [22].

At the laboratory scale, turbulent flow interactions with a three-bladed, 0.5 m diameter, horizontal axis hydrokinetic turbine and its turbulent wake are studied in Chamorro et al. [9]. Chamorro et al. [9] observed that the velocity deficit persists beyond 15 turbine diameters at hub height (10% velocity deficit at 15 diameters downstream) [9], and that wake recovery is enhanced by the higher shear in the top portion of the water column [9]. The authors also observed that the velocity deficit at hub height is related to the turbine's tip-speed ratio, since the extracted power is related to this parameter [1]. In terms of turbulence intensity, this turbine wake showed variability along the water column [9]. The higher levels of turbulence intensity were observed about 5 turbine diameters downstream of the turbine at the top portion of the wake (where the higher mean flow shear occurred in the wake), and it is reported that the increased turbulence intensity expands and reaches the free-surface about 15 diameters downstream of the turbine [9].

The wake structure and recovery processes differ between axial-flow turbines and cross-flow turbines, as previous investigations have shown that cross-flow turbines are more efficient in wake recovery than axial-flow turbines [19]. The near-wake of a vertical cross-flow turbine is assessed in Bachant and Wosnik [19]. The near-wake of Bachant and Wosnik [19] turbine is characterized by an asymmetric velocity deficit, high magnitude Reynolds stresses in the boundaries of the wake, and asymmetric turbulent kinetic energy (enhanced in the side corresponding to blade vortex shedding, were the minimum velocity deficit was found) [19]. Bachant and Wosnik [19] also identify the processes that contribute to faster wake recovery in cross-flow turbines by examining the terms in the stream-wise Reynolds-averaged Navier-Stokes (RANS) equation and in the kinetic energy balance. For their case, the authors found that wake recovery is dominated by the advection terms rather than by turbulence transport [19], which makes cross-flow turbines more efficient in entraining momentum into the wake when compared with axial-flow

[1] For general turbine characteristics and performance parameters refer to Burton et al. [23] and Batten et al. [24].

turbines [19].

The wake of a cross-flow turbine is investigated numerically in [15] by solving the Unsteady-RANS equations around a single rotating cross-flow blade in an unconfined channel. Strong deficit in all three velocity components was observed (60%), together with distinct direction patterns in vertical and cross-stream velocities. In the stream-wise direction, the wake expands both laterally and vertically, while the mean stream-wise velocity continuously increases downstream of the turbine, reaching an 85% recovery after 12 turbine diameters. Stream-wise velocity evolution downstream of the turbine is found to be dominated by cross-stream and vertical advection together with the stream-wise pressure gradient.

Despite the large amount of research regarding the turbine wake at the numerical and laboratory scales, there is a lack of field observations in real environments, probably due to the low number of full-scale turbines deployed around the world. However, field measurements are critical for validating numerical results and for scaling laboratory experiments results, as well as for estimating the true environmental effects of hydrokinetic energy extraction at each location.

This paper presents the first field observations of the wake from a full-scale hydrokinetic turbine under natural flow conditions. Specifically, a detailed characterization of Ocean Renewable Power Company (ORPC) RivGen turbine wake in the Kvichak river (Alaska) is reported. The site and turbine details together with the measurements methodology are presented in section 2. Section 3 presents a description of the wake in terms of mean flow and turbulence parameters. A discussion on the wake evolution, on the wake of a not-operational turbine, and on the wake energy loss is presented in section 4, followed by Conclusions in section 5.

2. Methods

2.1. Site and Turbine Description

The Kvichak river, located in southwest Alaska, drains the Iliamna Lake flowing southwest towards Bristol Bay. The turbine deployment site is about 2 km downstream from the Iliamna Lake, next to the village of Igiugig, where the river is approximately 5 m deep and 150 m wide. The flow is at is maximum, ~ 2.5 m/s, in the center of the river. Figure 1a shows a map of the Kvichak river bathymetry on top of a Google Earth image of the area, together with the location of the turbine deployment site: N 59° 19.495′; W 155° 54.890′.

The Ocean Renewable Power Company (ORPC) RivGen turbine is an horizontal cross-flow hydrokinetic turbine rated at 35 kW [25]. The turbine consists in two rotors plus a generator located in between the rotors. The entire turbine is 11.5 m wide, and each rotor is 1.5 m in diameter. Turbine hub-height at this location is approximately 2.5 m below the river free surface when the turbine is submerged and resting on the riverbed. Turbine blockage in the Kvichak river was estimated to be 10% when considering the turbine swept area plus the turbine's support structure area over the area of the river cross-section at the turbine location. Details of turbine performance in the Kvichak river can be found in the work of Forbush et al. [25]. A picture of ORPC RivGen sitting on top of the river free surface prior to its deployment is shown in Figure 1b.

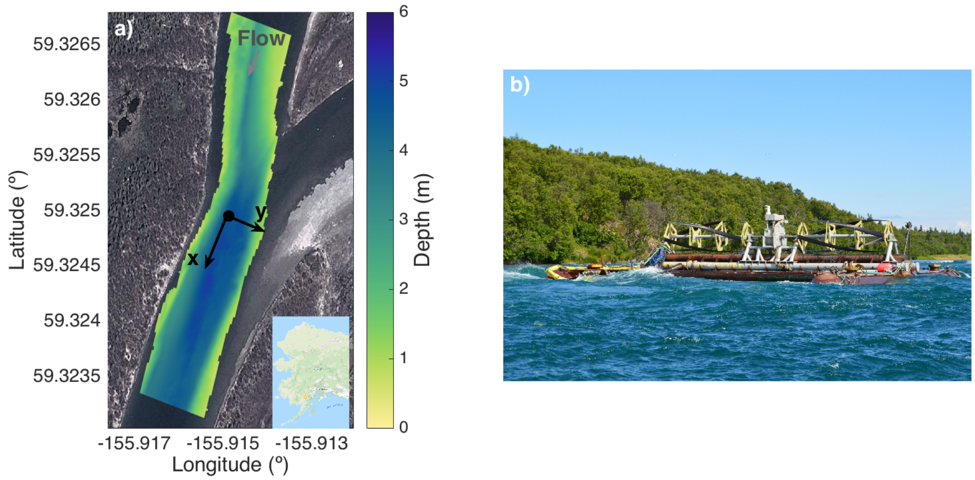

Figure 1: a) Google Earth image of the Kvichak river and river bathymetry in colors. Black dot shows turbine location, and black arrows identify the local coordinate system used through the wake analysis. Grey arrow represents the flow main direction. b) Downstream view of ORPC RivGen sitting on top of the Kvichak's river free surface prior to its submergence in July 2015.

2.2. Data Collection

Hydrodynamic data was collected in the area surrounding RivGen prior to and after its the deployment on July 2015. A new version of the SWIFT v4β drifter buoy [26] was used to measure surface velocity and velocity fluctuations along the water column (Figure 2). A summary of all instrument deployments and settings is presented in Table 1.

A Nortek Signature1000 five-beam acoustic Doppler current profiler (AD2CP) was mounted down-looking on a disk buoy, which was equipped with two Qstarz GPS data receivers. The Signature1000 measured along-beam velocities trough the water column as it was drifting using its five beams at 8 Hz in broadband mode. There were 14 depth bins separated by 0.5 m, and a 0.5 m blanking distance. Single ping error, σ_b, reported by the instrument manufacturer is 0.05 ms^{-1} for the along-beam velocities. The GPS measured geographic position, drifting velocity, and heading at 10 Hz, with a 5 m accuracy in position and 0.05 ms^{-1} in drifting velocity (using a phase-resolving GPS antenna).

Drifts began $\sim$ 200 m upstream of the turbine location by releasing the drifter from a small vessel. The drifter was released at different positions across the river in order to follow different surface streamlines across the river. After each drift, the SWIFT was recovered $\sim$ 200 m downstream of the turbine.

Two sets of drifts were conducted: before and after turbine deployment. The first set aimed to characterize the river in its undisturbed state. This data set consisted of 150 drifts between July 8th and July 13th, 2015. A portion of the drifts (15) were set-up to measure altimetry (bathymetry) with additional pings, and this restricted along beam velocity sampling to 4 Hz (instead of 8 Hz).

The second set of drifts was conducted after turbine deployment, from July 19^{th} to July 21^{st}, 2015. On July 19^{th} 2015, the turbine was underwater but not-operational (braked), while on July 20^{th} and 21^{st}, the turbine was operational and delivering electricity to the grid. There were 40 drifts while the turbine was not-operational, and 150 while it was operational. These data sets covered the same longitudinal river span as for the no turbine conditions, but concentrated drifts over and next to the turbine to evaluate the turbine wake. As for the first set, 25 drifts were taken in altimeter mode, measuring along-beam velocities at 4 Hz.

Data from the Signature1000 was quality controlled by removing measurements with low beam correlations (less than 30) and low echo amplitude (less than 80 dB). This process allowed to remove all data recorded while the SWIFT was outside of the water, and to recognize the riverbed.

An additional data set was obtained prior to turbine deployment using a Nortek Vector acoustic Doppler velocimeter (ADV) in order to provide ORPC with upstream turbine flow conditions and to test the accuracy of the drifting method measurements. The ADV was mounted on a turbulence torpedo (TT), a sounding weight that hangs from a davit on the aft of a small vessel while the vessel is holding station [27, 28]. The ADV targeted the turbine hub-height (2.5 m below river free surface) at several locations around the turbine site. Vessel location and drifting velocity were recorded using two Qstarz GPS located on top of the davit. The ADV sampled turbulent velocities at 16 Hz, for about 20 minutes at each targeted location.

Table 1: Summary of deployments and sampling parameters at the Kvichak river

Turbine State	No Turbine	No Turbine	Not Operational	Operational
Instrument	Nortek Vector	Nortek Signature 1000	Nortek Signature 1000	Nortek Signature 1000
Dates	8-13 July 2015	8-13 July 2015	19 July 2015	20-21 July 2015
Hold Stations/Drifts	35	150	40	150
Sampling Frequency (Hz)	16	8	8	8
z target (m)	-2.5	-	-	-
Δz (m)	-	0.5	0.5	0.5
Distance to first cell (m)	-	0.25	0.25	0.25
Range (m)	-	7	7	7
Single ping error (ms^{-1})	0.02	0.05	0.05	0.05

ADV data was quality-controlled to remove data with low correlation and low echo amplitude, and despiked using the 3D phase space method of Goring and Nikora [29]. The ADV data was organized in 1 minute ensembles and screened by vessel drifting velocity, where data with an ensemble-averaged vessel drifting velocity higher than 0.5 ms^{-1} were removed (not holding station). Additional motion contamination from the deployment platform was removed by applying the methods presented in [28].

In order to make the data sets comparable to each other for the analysis to follow, it is essential to assume steady state conditions (in the mean flow sense) in the Kvichak river during the measurements period. This assumption is evaluated in Appendix A.

2.3. Coordinate Systems

A local coordinate system is defined (shown in Figure 1) for data organization purposes, with x along the stream-wise direction, y in the cross-stream direction, and z in the vertical direction (positive upwards). The local coordinate system origin is at the free surface at the nominal center of the turbine

(N 59° 19.495′; W 155° 54.890′), and the local axis rotation from an east-north-up (true) coordinate system is 107° clockwise from north. The same coordinate system is used to define river velocities, with x corresponding to the stream-wise velocity u, y corresponding to the cross-stream velocity v, and z corresponding with the vertical velocity w. The location of each measurement, originally in latitude and longitude coordinates, is mapped to the local coordinate system.

Following the coordinate change, all data sets (including the data from the turbulence torpedo ADV) are organized by location in a three-dimensional structured uniform grid defined in the local coordinate system. The grid is of 2 m horizontal resolution, and 0.5 m vertical resolution (coincident with the Signature1000 velocity bins). The grid covered from -200 m to 200 m in x, from -60 m to 60 m in y, and from 0 m to -7 m in z. The ADV data set grid contained data only at $z = -2.5$m, corresponding to turbine hub-height.

Within each grid cell two data products are constructed: true Eulerian velocities and pseudo-beam velocities, which will be used in the coming sections to define river mean-flow and turbulence parameters, respectively.

2.3.1. True Eulerian Velocities

Velocities captured by the drifting Signature1000 correspond to fluctuations from the surface drifting velocity. All recorded velocities (from the GPS and from the Signature1000) are converted to east-north-up (ENU) velocities, and subsequently converted to velocities in the local coordinate system (u, v, and w). True Eulerian velocity profiles in the local coordinate system are constructed as:

$$u(x, y, z, t) = u_{GPS}(x, y, t) + u_{Sig}(x, y, z, t) \tag{1}$$

$$v(x, y, z, t) = v_{GPS}(x, y, t) + v_{Sig}(x, y, z, t) \tag{2}$$

where u and v correspond to the horizontal components of velocity in the local coordinate system, the GPS subscript represents drifting velocity components recorded by the GPS, and the Sig subscript represents velocity components recorded by the Signature1000. Vertical profiles of vertical velocities w do not need to be reconstructed as they are directly recorded by vertical beam of the Signature1000.

2.3.2. Pseudo-beam velocities

During these measurements, instrument horizontal rotation could not be controlled, thus the heading of the Signature1000 changed within each drift. Then, within each grid cell, the raw along-beam velocities recorded by the Signature1000 might not coincide with each other in direction, hence no time-series of along-beam velocities can be directly obtained. A fixed local system of four pseudo-beam velocities directions is defined within each grid cell to overcome this difficulty. In the new system, the horizontal component direction of each pseudo-beam velocity corresponds with the direction of the local coordinate system axis: the horizontal component of b_1 corresponds with the positive x-axis, the one from b_2 corresponds with the positive y-axis, the one from b_3 corresponds with the negative x-axis, and the one from b_4 corresponds with the negative y-axis direction. The pseudo-beam velocity coordinate system is shown in Figure 2b together with an example of the miss-alignment between the local-coordinate system and the Signature1000

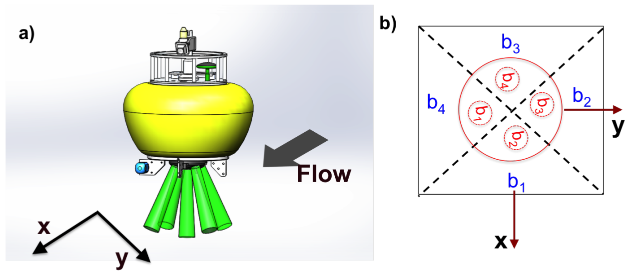

Figure 2: a) SWIFT v4 prototype schematic, rendered by Alex de Klerk (APL-UW). Green cone-shape areas illustrate the Nortek Signature1000 along-beam velocity directions. b) Plan-view of a single horizontal grid cell illustrating the pseudo-along beam velocities local system. In red is an example of miss-aligned along-beam velocities from the Signature1000.

along-beam velocities.

For every single measurement, the pseudo-beam velocities are constructed based on the heading recorded by the Signature1000, as the heading indicates the direction of the recorded along-beam velocities with respect to the local coordinate system. First, a heading with respect to the local x-axis is estimated as $H_x = H - 17°$, where H is the instrument heading and H_x is the local heading. When $H_x = 180°$, the instrument x-axis is aligned with the local x-axis. Four 90° angular cells, each centered in the directions of the local coordinate system axis, are defined within each grid cell and are used to classify four heading scenarios. Based on H_x, pseudo-beam velocities are defined as shown in Table 2.

2.4. Mean flow parameters

Mean flow parameters are obtained from the true Eulerian velocities estimated within each grid cell. These parameters are used to characterize and quantify the hydrodynamic effects of RivGen in the Kvichak river in the

Table 2: Pseudo-beam velocities based on instrument heading with respect to local coordinate system x-axis.

Pseudo-beam velocities	$135° < H_x < 225°$	$225° < H_x < 315°$	$315° < H_x < 45°$	$45° < H_x < 135°$
b_1	b_{1Sig}	b_{2Sig}	b_{3Sig}	b_{4Sig}
b_2	b_{2Sig}	b_{3Sig}	b_{4Sig}	b_{1Sig}
b_3	b_{3Sig}	b_{4Sig}	b_{1Sig}	b_{2Sig}
b_4	b_{4Sig}	b_{1Sig}	b_{2Sig}	b_{3Sig}

following sections.

At each grid cell, a non-uniform time-series of true Eulerian velocity components is available. Assuming steady state conditions in the Kvichak river during the field measurements (see Appendix A), these time-series are averaged in order to have a single velocity vector at each grid-cell. All velocity measurements are affected by the intrinsic noise of the instruments that measures them. For this case, the velocity measurements are affected by the GPS velocity uncertainty and by the inherent Doppler noise of the Signature1000. After time-averaging the velocities, the horizontal velocity components uncertainty within each grid cell, σ_u, is defined as:

$$\sigma_u = \sqrt{\frac{\sigma^2_{u_{Sig}}}{N} + \frac{\sigma^2_{u_{GPS}}}{N}} \tag{3}$$

where $\sigma_{u_{Sig}}$ is the horizontal velocity uncertainty from the Signature1000, $\sigma_{u_{GPS}}$ is the uncertainty of the velocity recorded by the GPS on board the SWIFT buoy, and N is the number of velocity measurements available within each grid cell.

Using the time-averaged velocity vector at each grid cell, velocity shear is estimated by a centered finite difference scheme. A coarse vorticity is then estimated using the estimated discrete shear in all three Cartesian directions. The shear of the along-channel velocity component u in the x direction, and its uncertainty are defined as:

$$\frac{du}{dx} = \frac{u_{i+1,j,k} - u_{i-1,j,k}}{2\Delta x} \tag{4}$$

$$\sigma_{Shear} = \frac{1}{2\Delta x}\sqrt{\sigma^2_{u_{i+1,j,k}} + \sigma^2_{u_{i-1,j,k}}} \tag{5}$$

Where i, j, and k represent each grid cell, u is the x-axis velocity component, and σ_u is the velocity component uncertainty previously defined in Eq. 3. The velocity shear in the other directions, and for the rest of the velocity components (v and w), follows the same definition.

Additional mean flow parameters uncertainties arise from the error in the GPS measurements location and from natural variability within a grid-cell. These are assumed to be uncorrelated, and thus averaging within the grid-cells significantly reduce them.

2.5. Turbulence Parameters

Turbulence parameters are obtained following the same methods presented in [30] for a 5-beam acoustic Doppler profiler, which are based on the variance of along-beam turbulence fluctuations. For this investigation, the pseudo-beam velocity fluctuations are used instead.

A pseudo-turbulence intensity (TI) is estimated using the pseudo-beam velocity variances, $b_i'^2$, relative to the mean flow velocity at each depth. The noise-corrected pseudo-TI, pTI, is defined as:

$$pTI(x,y,z) = \frac{\sqrt{\frac{1}{5}\sum_{i=1}^{5} b_i'^2(x,y,z,t) - \sigma_b^2}}{U(x,y,z)} \tag{6}$$

where b_i represents each pseudo-beam velocity, σ_b^2 is the along-beam velocity noise variance removed following [31], and U is the horizontal velocity magnitude. The pseudo-beam measurements have independent noise errors, σ_b, and thus the use of all five pseudo-beam velocities is preferred to estimate the velocity variations at each grid cell. By only using the pseudo-beam velocities, pseudo-TI only captures the turbulent length scales similar to the beam separations. This spatial definition is uniformly biased low compared to the usual temporal definition of turbulent intensity $\sigma_U/\bar{U}$, where σ_U is the standard deviation of the flow velocity and $\bar{U}$ corresponds to the mean flow velocity.

The five-beam configuration of the Signature1000 allows for the estimation of five out of six Reynolds stresses [30]. Assuming zero-mean pitch and roll within each grid cell, the noise corrected Reynolds stresses are defined using the variance of the pseudo-beam velocity fluctuations as:

$$\overline{u'^2} = \frac{\overline{b_1'^2} + \overline{b_3'^2} - 2\overline{b_5'^2}\cos^2\theta}{2\sin^2\theta} - \sigma_b^2 \tag{7}$$

$$\overline{v'^2} = \frac{\overline{b_2'^2} + \overline{b_4'^2} - 2\overline{b_5'^2}\cos^2\theta}{2\sin^2\theta} - \sigma_b^2 \tag{8}$$

$$\overline{w'^2} = \overline{b_5'^2} - \sigma_b^2 \tag{9}$$

$$\overline{u'w'} = \frac{\overline{b_3'^2} - \overline{b_1'^2}}{4\sin\theta\cos\theta} \tag{10}$$

$$\overline{v'w'} = \frac{\overline{b_4'^2} - \overline{b_2'^2}}{4\sin\theta\cos\theta} \tag{11}$$

where $\overline{b_i'^2}$ corresponds to the pseudo-beam velocity variances, and θ is the beam inclination angle (25° for the Signature1000), and σ_b^2 corresponds to the noise variance from the Signature1000. The $\overline{u'^2}$ corresponds to the along-channel turbulent kinetic energy (TKE), which can be used to estimate an along-channel turbulence intensity as:

$$TI(x,y,z) = \frac{\sqrt{\overline{u'^2}}}{U(x,y,z)} \tag{12}$$

Both the along-channel turbulence intensity and the along-channel TKE will be used here as a measure of how the turbulence is increasing and how is it evolving downstream of the turbine.

The turbulent kinetic energy dissipation rate is estimated through the second-order spatial function of the along-beam velocity fluctuations $D(z,r)$, following the methodology described in [32] and [30]. This methodology requires the observation of the inertial sub-range of isotropic turbulence. Using the vertical beam velocity fluctuations, within each grid cell the structure function is defined as:

$$D(z,r) = \overline{\left(b_5'(z+r) - b_5'(z)\right)^2} \tag{13}$$

where z is the along-beam measurement location, b_5' corresponds to the velocity fluctuation along the vertical beam, and r is the distance between two velocity bins; the overline denotes a time-average. In the inertial subrange of isotropic turbulence, the structure function is related to the distance r and to the TKE dissipation rate ϵ by:

$$D_i(z,r) = C_v^2 \epsilon^{2/3} r^{2/3} \tag{14}$$

where C_v^2 is a constant equal to 2.1 [32, 31].

The structure function is estimated using all instantaneous profiles within each grid cell (which correspond to a non-uniform time series). Then, the structure function is multiplied by $r^{-2/3}$ to obtain a compensated structure function in the inertial subrange [33]. The dissipation rate is estimated by solving $\overline{D(z,r)r^{-2/3}\big|_{r_1}^{r_2}} = C_v^2 \epsilon^{2/3}$, where r_1 to r_2 is the range where the compensated structure function slope is closest to zero, and the overline denotes an average. Estimates are not calculated for depths with less than four points in the structure function, hence r values ranged between 2 m and 7 m.

Uncertainties in TKE dissipation rates from the structure function fitting are calculated by propagating the uncertainty in the compensated structure function, such that:

$$\sigma_{\epsilon_D} = \left(\frac{1}{Cv^2}\right)^{3/2} \frac{3}{2} \overline{D_{comp}}^{1/2} \sigma_{D_{comp}} \tag{15}$$

where $\sigma_{D_{comp}}$ corresponds to the standard deviation of the compensated structure function in the r range used for the computations.

2.6. Data-products comparison

Flow parameters obtained from the SWIFT data set are compared with those obtained from the ADV data set for the no-turbine river conditions in order to test the accuracy of the drifting method. Data are compared in terms of the velocity magnitude, pseudo turbulence intensity, turbulence intensity, and TKE dissipation rate. ADV-based flow parameters are obtained similarly to those from the SWIFT buoy, with the exception of TKE dissipation rate, which is estimated through the TKE spectra estimated from the

ADV measurements following the method presented in [30]. Figure 3 shows a comparison of the grid cell flow parameters (in blue), together with grid longitudinal averages (in grey) as longitudinal homogeneity was observed in the area covered by the ADV measurements.

Overall there is a good agreement between flow parameters obtained by the drifting method and the station-keeping method. An excellent agreement is observed for the gridded velocity magnitude between both measurement methods, with an $RSME = 0.16$ ms^1 between the values from the SWIFT and the values from the TT-ADV platform. Good linear agreement is found between the pseudo-turbulence intensity from both data sets, however the pseudo-turbulence intensity from the SWIFT data set is biased low. This bias is expected, since the pTI only considers a portion of the turbulence length-scales, while the turbulence intensity from TT-ADV is estimated by its usual definition and considers all turbulence length-scales in the along-channel direction. The plot in panel (c) shows turbulence intensity estimated as in Eq. 12. Although significant scatter in the plot is observed, a linear trend and good agreement is found between the longitudinal averages. The dissipation rate estimates from the TT-ADV tends to be larger than those from the SWIFT. Despite the scatter in the comparison of these turbulence parameters, the average values obtained from the two methods lie in the same order of magnitude. This is notable, given the large dynamic range of this quantity in the natural environment.

Differences might be explained by uncertainties in the location of the measurements (from the GPS receivers), by remaining noise in the parameters estimates, and by differences in the calculation methods. Specifically, the station keeping provides highly populated time series of flow parameters within each grid cell, while the drifter methods provides spatial averages obtained through averages of non-uniformly sampled data.

3. Results: Wake Characterization

The RivGen wake in the Kvichak river is characterized by the previously defined flow parameters obtained from the repeated SWIFT drifts. In general, the wake signal is strong and noticeable in all estimated flow parameters. In what follows the river original flow conditions and post-turbine deployment flow conditions are presented, always considering an operational RivGen. (The braked, non-operational RivGen will be considered in the Discussion.) Horizontal and longitudinal views of the river are presented, colored by the different mean flow and turbulence parameters. All horizontal view maps correspond to hub-height ($z = -2.5$m), while longitudinal views correspond to a streamline passing through the center of the turbine shown as a gray dotted-line in Figure 4b.

3.1. Mean flow parameters

Figure 4a shows contours of grid-averaged velocity magnitude at hub-height for a undisturbed river conditions. The flow is stronger mid-river, reaching about 2.3 ms^{-1} at the turbine location ($(x, y) = (0, 0)$), while slower flows are observed towards the river banks. When the river is undisturbed, strong lateral shear is observed at the cross-section corresponding with the turbine location, showing stronger flows towards the Igiugig side of the river (positive y-axis).

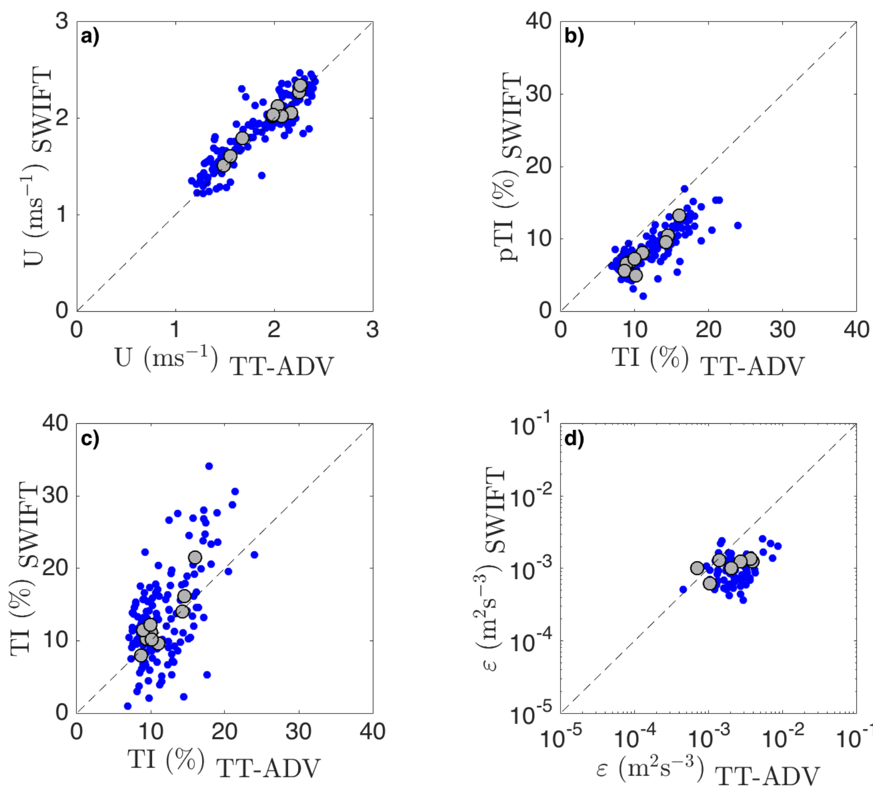

Figure 3: Comparison of flow parameters between ADV data (x-axis) and SWIFT data (y-axis) for the no turbine river condition: a) Velocity magnitude, b) pseudo-turbulence intensity, c) turbulence intensity, and d) TKE dissipation rape. Blue dots correspond to grid cell parameters, and gray larger dots correspond to longitudinal averages of grid cell values. Dotted line corresponds to the $y = x$ in all plots.

A plan view of velocity magnitude at hub-height while the turbine is operational is presented in Figure 4b. The turbine wake is observed immediately downstream of the turbine. Velocity magnitude is dramatically reduced, from 2.3 ms^{-1} to 1 ms^{-1} at the turbine location, and slower velocities are observed beyond 200 m downstream of the turbine. The wake remains mostly laterally constrained by the natural shape and direction of the river. Closer to the free-surface (above hub-height), the wake from the two turbine rotors can be distinguished, together with a reduced wake from the generator (located between the two rotors). These features are mixed about 40 m downstream of the turbine.

Figure 5 shows a longitudinal profile of the river colored by velocity magnitude. In its undisturbed state, classical boundary layer flow is observed in the river, with velocities increasing from the bottom towards the free-surface. The turbine wake has a rich longitudinal structure. The velocity decrease is observed to begin upstream of the turbine, as the river flow encounters an obstacle (the turbine) and slows down. On top of the turbine, faster flow is observed, consistent with acceleration on top of an obstacle. At this centerline longitudinal view, flow also accelerated bellow the turbine rotor, suggesting important vertical blockage effects. During the field measurements, a small free-surface decrease was observed at the turbine location, but is not captured by the vertical motion of the drifter.

Downstream of the turbine the wake expands vertically, reaching the free-surface about 35 m away from the turbine, where the wake is also observed in the surface velocities recorded by the GPS on board the SWIFT buoy.

Average uncertainty in the velocity estimates previous to turbine deploy-

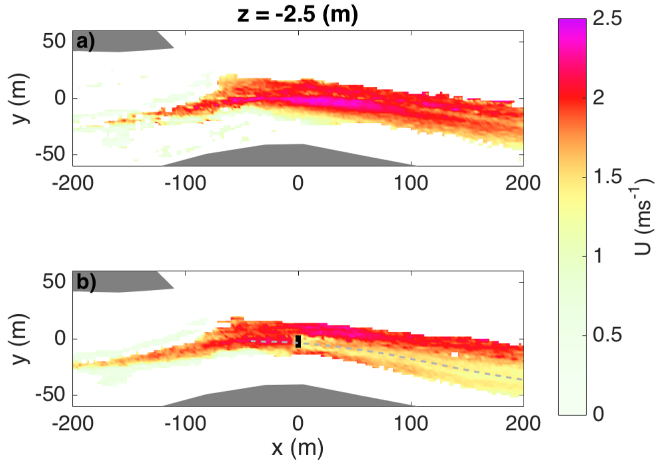

Figure 4: Plan view of horizontal velocity magnitude at hub-height (2.5 m below river free surface). a) Before turbine deployment, and b) when turbine is underwater and operational. Flow is from left to right in both plots. Grey dashed line in a) shows location of center streamline used for the longitudinal plots.

ment is 1.3 cms^{-1}, and 1.2 cms^{-1} when the turbine is operational.

In its natural state, the Kvichak river shows a vertical vorticity (ω_z) of opposite direction along the Igiugig side of the river (positive y-axis), probably due to a lateral sharp change in bathymetry (Figure 6a. The underwater presence of the turbine has a strong impact on vertical vorticity, generating enough vertical vorticity to reverse its original sign right at the lateral edges of the turbine, showing the expected behavior for an obstacle present in the flow (Figure 6b. Cross-stream vorticity, ω_y, is shown in Figure 7. Baseline cross-stream vorticity shows a maximum near the bottom, consistent with bottom-induced vorticity. Similarly, when the turbine is underwater, cross-stream vorticity is enhanced on top and below the turbine, and vorticity direction is coincident with increased vorticity observed in flow passing around

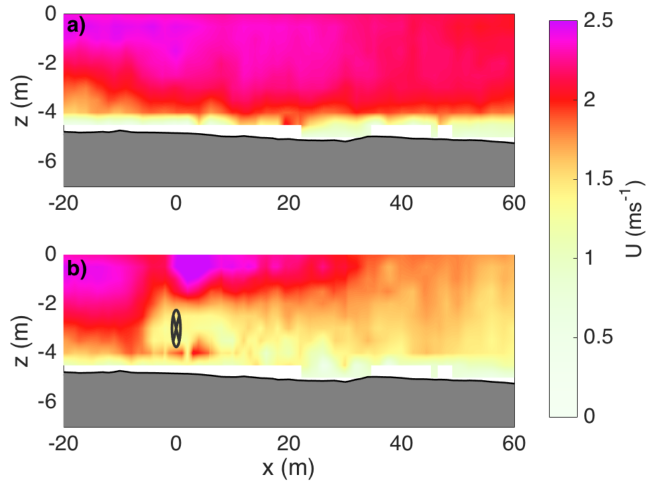

Figure 5: Longitudinal view of horizontal velocity magnitude along a center streamline (shown in Figure 3a). a) Before turbine deployment, and b) when turbine is underwater and operational. Flow is from left to right in both plots.

a cylinder. However, the wake vorticity magnitude is asymmetric, similar to what was observed in laboratory experiments by [19]. This asymmetry might be explained by blade rotation, which induces cross-stream vorticity of opposite direction. For the not-operational condition, cross-stream vorticity bellow the turbine, is of similar magnitude than cross-stream vorticity observed on top of the turbine. Average uncertainty is 0.04 s^{-1} for the vertical vorticity and 0.1 s^{-1} for the cross-stream vorticity.

3.2. Turbulence Parameters

Maps of turbulence intensity (TI) estimated as the ratio between the standard deviation of the along-channel turbulence fluctuations and the along-channel velocity are shown in Figures 8 and 9. Previous to turbine deployment, river TI is about 10% through the water column. Larger values of TI

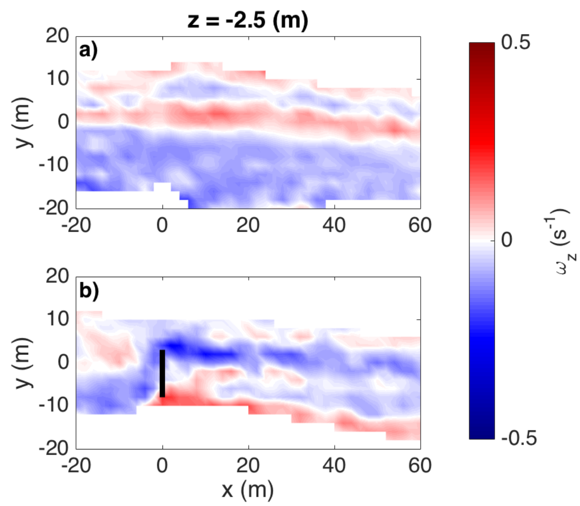

Figure 6: Plan view of vertical vorticity ω_z at hub-height (2.5 m below river free surface). a) Before turbine deployment, and b) when turbine is underwater and operational. Flow is from left to right in both plots.

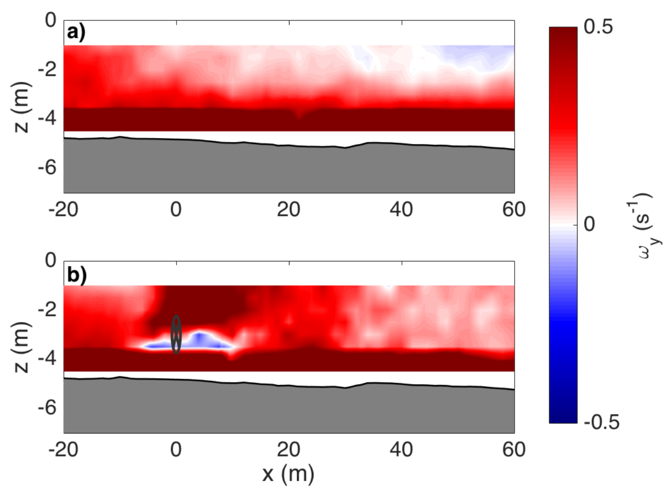

Figure 7: Longitudinal view of cross-channel vorticity ω_y along a center streamline (shown in Figure 3a). a) Before turbine deployment, and b) when turbine is underwater and operational. Flow is from left to right in both plots.

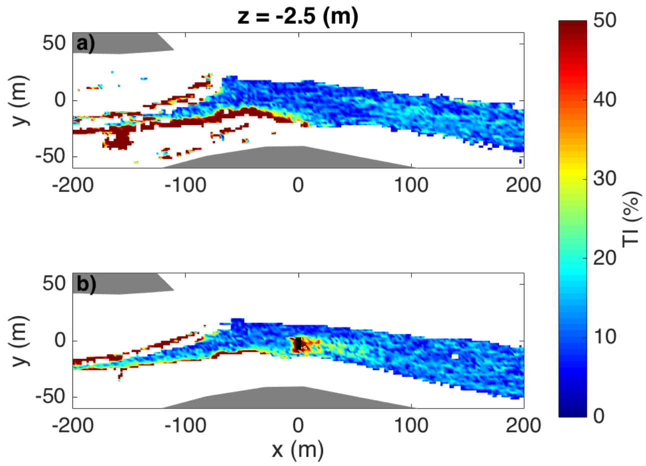

Figure 8: Plan view of total turbulence intensity at hub-height (2.5 m below river free surface). a) Before turbine deployment, and b) when turbine is underwater and operational. Flow is from left to right in both plots.

are observed near the bottom and in the shallower areas of the river, consistent with bottom-generated turbulence and slower flows. When the turbine is deployed, a region of elevated TI is observed in the area surrounding RivGen. TI increases more than 5 times from its original level due to both an increase in velocity fluctuations (up to 5 times) and a decrease in mean velocity. Unlike the mean velocity, the turbulence intensity, and the TKE, decrease rapidly downstream of the turbine, reaching a level similar to the natural river conditions. As shown in the plan-view plot of Figure 8b, the wake in terms of turbulence intensity decreases its width, concentrating the elevated TI towards mid-river.

The turbine effects are also observed in the Reynolds stresses, which are representative of turbulent momentum transport in the wake. Although es-

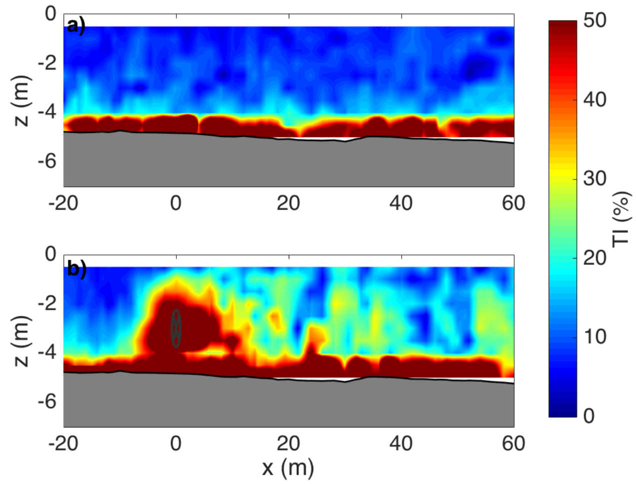

Figure 9: Longitudinal view of turbulence intensity along a center streamline (shown in Figure 3a). a) Before turbine deployment, and b) when turbine is underwater and operational. Flow is from left to right in both plots.

timates are noisy, elevated Reynolds stresses are observed up to 20 m downstream of the turbine, suggesting that turbulent transport is of importance in this region. Figures 10 and 11 show contour maps of the $\overline{u'w'}$ Reynolds stress. The regions of strong $\overline{u'w'}$ correspond with regions of velocity shear, which are caused by the decrease in velocity, and the net effect is consistent with higher TKE production.

TKE dissipation rate maps are shown in Figure 12 and 13. Right downstream of the turbine, TKE dissipation rate increases by at least a decade, consistent with the increase in turbulent kinetic energy. Along the center streamline, TKE dissipation rate is elevated through the entire water column. Although TKE dissipation rate decreases downstream of the turbine, it remains above baseline values at least for 60 m downstream of the turbine.

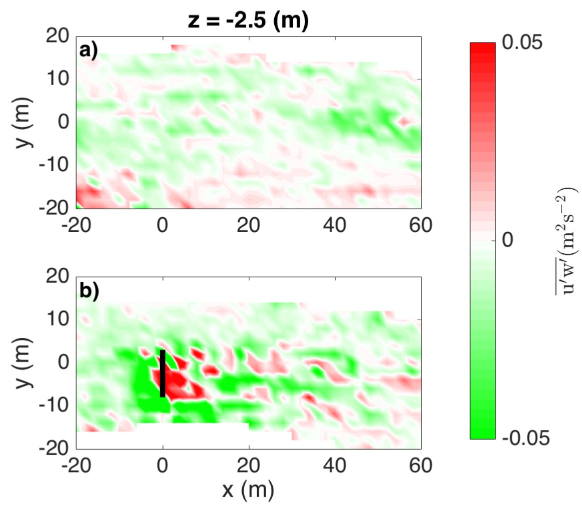

Figure 10: Plan view of $\overline{u'w'}$ Reynolds stress at hub-height (2.5 m below river free surface). a) Before turbine deployment, and b) when turbine is underwater and operational. Flow is from left to right in both plots.

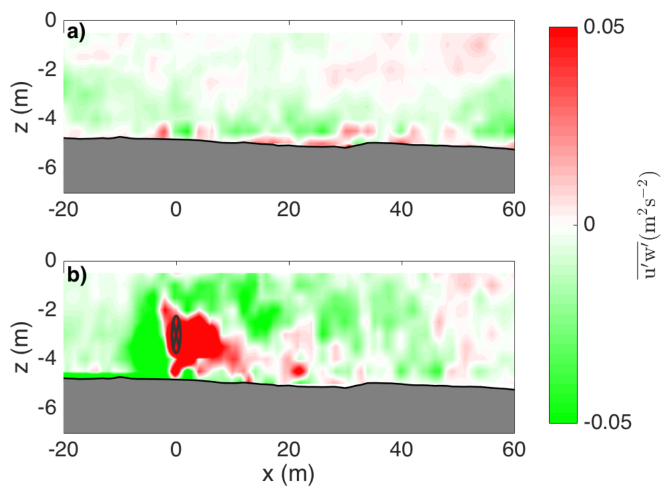

Figure 11: Longitudinal view of $\overline{u'w'}$ Reynolds stress along a center streamline (shown in Figure 3a). a) Before turbine deployment, and b) when turbine is underwater and operational. Flow is from left to right in both plots.

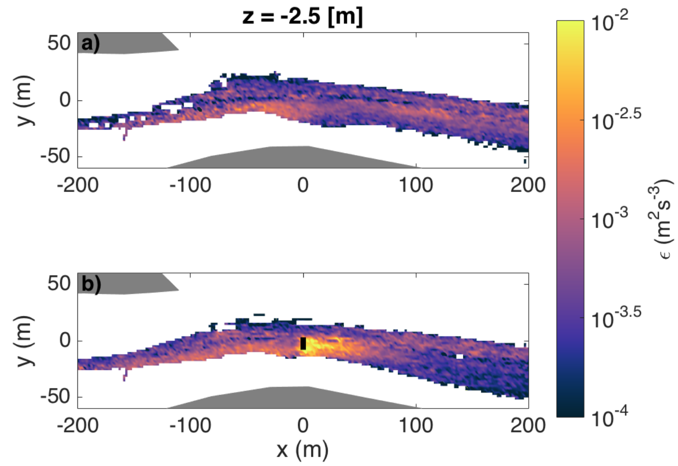

Figure 12: Plan view of TKE dissipation rate ε at hub-height (2.5 m below river free surface). a) Before turbine deployment, and b) when turbine is underwater and operational. Flow is from left to right in both plots.

Average uncertainty in the TKE dissipation rate estimates is 4.4×10^{-4} m^{2}s^{-3} prior to turbine deployment, and it is 7.6×10^{-4} m^{2}s^{-3} when the turbine is operational.

4. Discussion

4.1. Wake Evolution

Figure 14 compares horizontal and vertical profiles of velocity at different distances from the turbine for the river in its natural conditions and while the turbine is operational. Horizontal profiles, taken at hub-height, show the strong wake signal from the two rotors and the generator. The profiles slowly mix horizontally, however the wake signal is still clearly observed about 50 m downstream of the turbine. Vertical profiles, taken along the center stream-

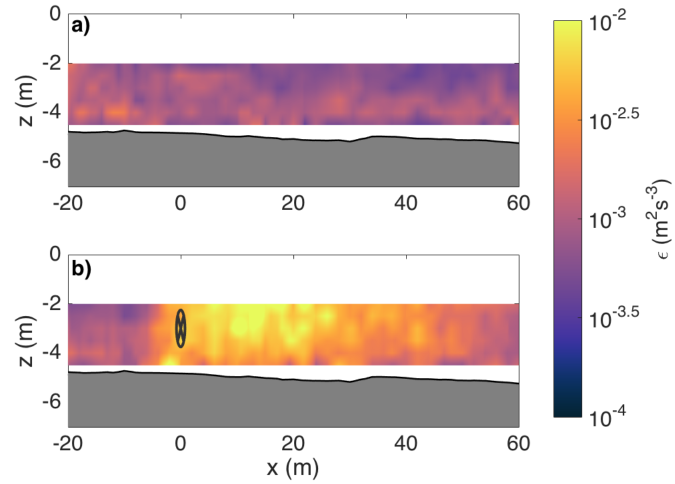

Figure 13: Longitudinal view of TKE dissipation rate ε along a center streamline (shown in Figure 3a). a) Before turbine deployment, and b) when turbine is underwater and operational. Flow is from left to right in both plots.

line shown in Figure 4b, show the sharp decrease in velocity at hub-height. Closer to the turbine, at $x = 2$ m, the velocity vertical profile shows the accelerated flow on top of the turbine. Vertically, the velocity profiles mix around 50 m downstream of the turbine, where typical boundary-layer profiles are observed. However, velocity remains slower when compared with the original vertical profiles due to energy extraction. These differences suggest that in this shallow river the velocity profiles homogenize faster vertically than horizontally, probably due to bottom-induced shear stress.

In what follows, the along-channel TKE ($\overline{u'^2}$) is used to study the wake evolution instead of turbulence intensity, since it provides information about the turbulence evolution rather than a ratio to the mean flow.

Longitudinal profiles of hub-height velocity (U), along-channel TKE ($\overline{u'^2}$),

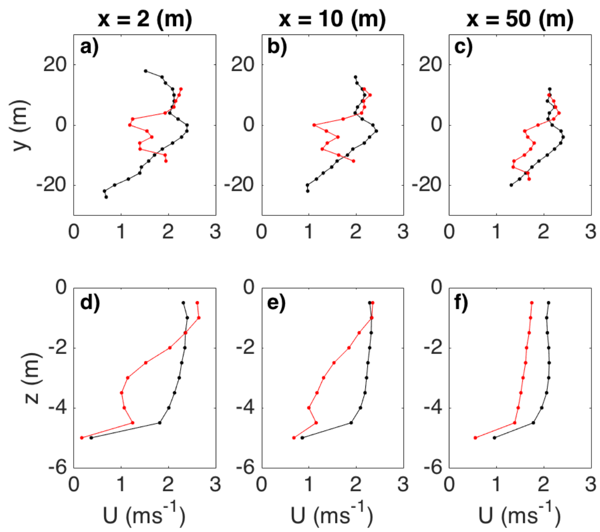

Figure 14: Horizontal and vertical profiles of velocity magnitude at three different locations downstream of the turbine. In black when there is no turbine in the water, and in red when the turbine is underwater and operational.

and TKE dissipation rate (ε), are presented in Figure 15. In these plots, the lines in dark colors represent an average between three streamlines: along the turbine port side, along the turbine center (shown in Figure 4), and along the turbine starboard side. Shadows represent the standard deviation from the averages between the three streamlines (a wider shadow indicates a large variation between streamlines).

Prior to turbine deployment, strong lateral shear was observed at hub-height at the turbine location, with stronger flow towards the turbine's starboard side and slower flow towards the turbine's port side. When the turbine is underwater and operational no significant lateral shear is observed just upstream of the turbine location. In the first 10 m of the wake, flow velocity is similar along the three streamlines. After 10 m downstream of the turbine, flow at the center and starboard streamlines increases slightly more than at the port side, which might be explained by the stronger flows observed in the starboard side outside of the wake. However, the flow velocities do not recover to their baseline conditions along any of the three streamlines, and any increase in velocity is very small.

Along-channel TKE is observed to have a similar behavior along the three streamlines. Along-channel TKE begins to increase about 10 m upstream of the turbine, reaching a peak around turbine location. In the first 20 m downstream of the turbine a rapid along-channel TKE decrease is observed. TKE increases again along the starboard streamline around $x = 15$m, which might be explained by additional TKE being produced in the edges of the wake. TKE fluctuations further downstream might be explained by river bathymetric features.

TKE dissipation rate shows a behavior that consistent with the increase in TKE. It begins to increase at the same time as the turbulent kinetic energy, and it peaks about 5 m downstream of the turbine, however it slowly decreases towards its original level about 60 m downstream of the turbine.

From Figure 15, three dynamic regions can be distinguished through the turbine influence. From $x = -10$ m to the turbine location at $x = 0$ m, a bow wake is observed, where velocity is decreasing while TKE is rapidly increasing. This region is followed by a near wake up to about $x = 10$ m, where velocity continues to decrease followed by a small amount of recovery, while TKE decreases constantly, and TKE dissipation rate reaches its peak. A far wake is observed beyond $x = 10$ m, where both velocity and TKE do not change significantly; the velocity deficit persists, TKE remains

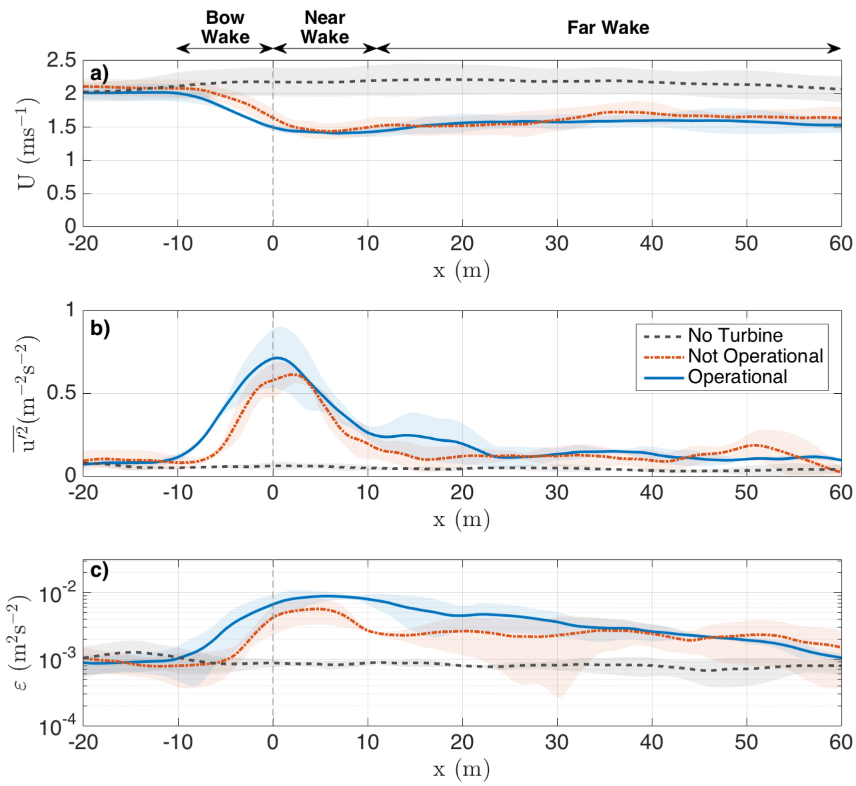

Figure 15: Hub-height longitudinal profiles of a) Velocity, b) Along-channel TKE, and c) TKE dissipation rate, for different river conditions. No turbine in gray, not-operational turbine in red, and operational turbine in blue. Darker lines correspond to a cross-stream average between three streamlines along the turbine wake (turbine port, center, and starboard sides). Lighter color shadows represent one standard deviation from the averages along the three streamlines.

slightly elevated with respect to its original level, and TKE dissipation rate continuously decreases. The far wake is an important demonstration that there is no true 'recovery' of the flow after this or any turbine, because kinetic energy has been extracted from the system. Of course, in some systems potential energy may be converted to kinetic energy, but the total energy is still reduced by extraction.

4.2. Not operational turbine

The wake observations shown in Section 3 correspond to the operational turbine conditions. During the life span of any hydrokinetic turbine it is expected that turbines will not be operational for periods of time, due to flow conditions not suitable for energy extraction, due to the presence of fauna, or due to maintenance, among other reasons. Here, the differences between the wake between the operational and not-operational turbine conditions are examined. Figure 15 presents longitudinal hub-height profiles for the three studied river conditions: no turbine, not-operational turbine, and operational turbine. When the turbine is not-operational the bow-wake shifts towards the turbine, and velocity reaches its minimum later in the profile, at $x = 8$ m instead of at $x = 2$ m for when the turbine is operational. Downstream, no significant differences are observed between both velocity profiles. A similar trend is observed in the TKE profiles, for the not-operational condition the TKE increases later in the profile, the TKE maximum is shifted downstream and it is of less magnitude than for the operational turbine condition. These differences are explained by both, turbine rotation and turbine energy extraction. Turbine rotation introduces additional turbulence and modifies the flow turbulence length-scales, resulting in a higher TKE level.

For the not-operational condition, the TKE dissipation rate also increases at the turbine location, after a small decrease about 10 m downstream of the turbine. On average, the dissipation rate remains elevated through the longitudinal extent of the wake, although large cross-wise variations are observed.

The small differences observed in the flow parameters between operational and not-operational conditions suggest that the turbine presence as a bluff body in the flow (as opposed to an extractor) is responsible for most of the hydrodynamic impacts in the Kvichak river.

4.3. Wake energy loss

The Kvichak river naturally looses energy through the dissipation of turbulent kinetic energy into heat and sound. When the turbine is underwater and operational, it extracts energy from the mean flow and delivers it to the local Igiugig grid. At the same time more turbulence is generated in the river due to the presence of the turbine and blade rotation. As more turbulence is generated, an increase in TKE dissipation rate is observed in the wake of RivGen. Thus, the river is loosing additional energy through the turbine wake. Here, a volumetric TKE dissipation rate is calculated by multiplying the TKE dissipation rate, ε, by the water density, ρ, and then integrated over the river volume (V) to obtain the rate at which energy is being loss to turbulence as:

$$\text{Rate of Energy Loss} = \int_V \rho \varepsilon dV \tag{16}$$

Wake energy loss rate for the three studied conditions is presented in Table 3. Total energy loss rate is calculated in a volume that covers most of

Table 3: River energy loss rates from turbine extraction and through dissipation of turbulent kinetic energy. Uncertainties are included for the turbulent dissipation values.

Condition	No turbine	Not operational turbine	Operational turbine
Turbulent Dissipation (kW)	3.43 ± 0.04	6.14 ± 0.16	10.93 ± 0.15
Turbine Extraction (kW)	-	-	9.9
Total (kW)	3.43	6.14	20.8

the turbine wake: between $x = 0$ m and $x = 60$ m, $y = -14$ m and $y = 14$ m, and from the bottom to the free-surface. Energy loss in the wake area doubles when the turbine is underwater, but not operational, and triplicates when the turbine is operational. Wake energy loss is comparable to what the turbine is delivering to the grid, which means that the river is loosing as much as two times the energy that is actually being delivered to the community. This amount of energy loss must be considered in the assessment of large hydrokinetic energy farms, as it indicates that a much larger effect on the hydrodynamics of a system exists in addition to what is being extracted by the turbine for electricity production alone.

5. Conclusions

Detailed field measurements are used to analyze and understand the evolution of the wake of ORPC RivGen hydrokinetic turbine in the Kvichak river. A drifting Nortek Signature1000 5-beam acoustic Doppler current profiler is used to measure along-beam velocities at high resolution following river streamlines. These observations are then used to construct a set of 3D flow conditions in the area surrounding the RivGen turbine for both before turbine deployment and while the turbine is underwater extracting energy.

In general, results show the expected wake characteristics of decreased velocities and increased turbulence downstream of the turbine, however unique wake features are observed.

A persistent velocity decrease is observed from 10 m upstream of the turbine extending more than 200 m downstream of the turbine (beyond the area covered measurements). Vertical blockage by the turbine is of importance, as the flow shows acceleration below and on top of the turbine. In terms of velocity, the wake slowly expands laterally, but rapidly expands vertically, reaching the free-surface about 35 m downstream of the turbine. The two-rotor wake signal is observed through the measurements in horizontal profiles of along-channel velocities, while vertically the velocity profiles homogenize about 50 m downstream of the turbine, while still experiencing lower velocities.

In terms of turbulence parameters, a rapid increase in turbulence intensity, and in turbulent kinetic energy, is observed, which peaks at the turbine location and then decreases downstream of the turbine. The increase in turbulence is consistent with an increase in TKE dissipation rate, which peaks later in the longitudinal profile and remains elevated through the extent of the measurements. Stronger Reynolds stresses near the turbine in areas of strong shear are also observed suggesting additional TKE production. In addition to velocity and turbulence, the turbine also affects river vorticity, inverting its natural direction to be in accordance with vorticity generated by a bluff body in a rapid flow for both lateral and vertical vorticity.

Similar patterns of velocity and turbulence are observed in the wake of a non-operational RivGen, with no large differences between the decrease in velocity and increase in turbulence parameters. This comparison suggest that the main hydrodynamic effects in the Kvichak river are due to the presence of the turbine and not due to blade rotation.

The TKE dissipation rate parameter allows for the estimation of total energy being loss by turbulence in the wake region. For the operational condition, the river looses about 11 kW in the wake area, which is comparable to what the turbine is delivering to the grid (10 kW in average during the field measurements period).

This study provides the first comprehensive data set of a full-scale cross-flow turbine wake. The methods used in the field are proved to be efficient in characterizing the spatial extent of the wake, at least in system that is in steady state for long periods of time. The observations and analysis presented here serve as validation for numerical models and for future turbine array designs. But most importantly these results inform turbine designers, project developers, and decision makers about the environmental impacts of hydrokinetic energy extraction under real flow conditions.

All data sets produced for this paper are available in the US Department of Energy Marine and Hydrokinetic Energy data repository website [2].

Acknowledgements

The authors thank the support of Joe Talbert, Alex deKlerk, Dylan Dubuque from APL-UW, Sam Harding from PNNL, Eric Nelson from NREL, the people from the village of Igiugig, and the Ocean Renewable Power Com-

[2]https://mhkdr.openei.org/home

pany for their help, support and collaboration in this project. This investigation is supported by the US Department of Energy (Award DE-EE0006397) and the Naval Facilities and Engineering Command (Award N00024-10-D-63). Maricarmen Guerra also thanks the support of Fulbright and Becas Chile - Conicyt doctorate fellowship programs.

Appendix A. Steady State Assumption

It is critical for the wake analysis presented here to assume steady state conditions in the Kvichak river. During the measurements period atmospheric conditions were mild and no large rain or flood events were observed. Since there are no stream flow gauges available in the Kvichak river, the steady state assumption is tested using velocity measurements taken upstream of the turbine location through the entire measurement period, and depth variations taken just upstream of the turbine while the turbine was underwater.

True Eulerian velocities taken mid-river between 20 and 30 m upstream of the turbine (within four highly populated grid cells) are used to test the steady state assumption through the measurements period. There were 1054 instantaneous velocity measurements within this location among 9 days of measurements. Turbulent velocities together with daily averages measured at hub-height at this location are shown in Figure A.16. Error bars correspond to one standard deviation from the daily averages. No trend is observed in the daily averaged velocities, and the total averaged velocity from those measurements lies within the error bars through the measurement period.

Data from a HOBO pressure gauge installed on RivGen's frame, just upstream the turbine, are converted to water depth after removing the atmospheric pressure data. Atmospheric pressure measured at the Igiugig Airport weather station (USAF-703061) during the measurements period is shown in Figure A.16a. During the first period of measurements (no turbine in the river), atmospheric pressure remained fairly constant at around 100 kPa. Increased atmospheric pressure was observed during the not-operational turbine measurements and for the first day of the operational turbine measurements. The effective accuracy from the HOBO pressure gages is 3 cm in depth. The water depth data presented in Figure A.16c shows no significant trend. However, high-frequency depth variations between ± 5 cm, over a 3.66 m mean depth were observed on July 19-21 2015.

Although there is variability in the flow conditions during the measurements, the steady-state assumption is statistically valid (i.e., none of the variations in the mean values exceed the uncertainties) during the entire measurement period. Furthermore, the upstream variations of order 0.1 ms^{-1} and much smaller than the wake signal, which is order 0.5 ms^{-1}.

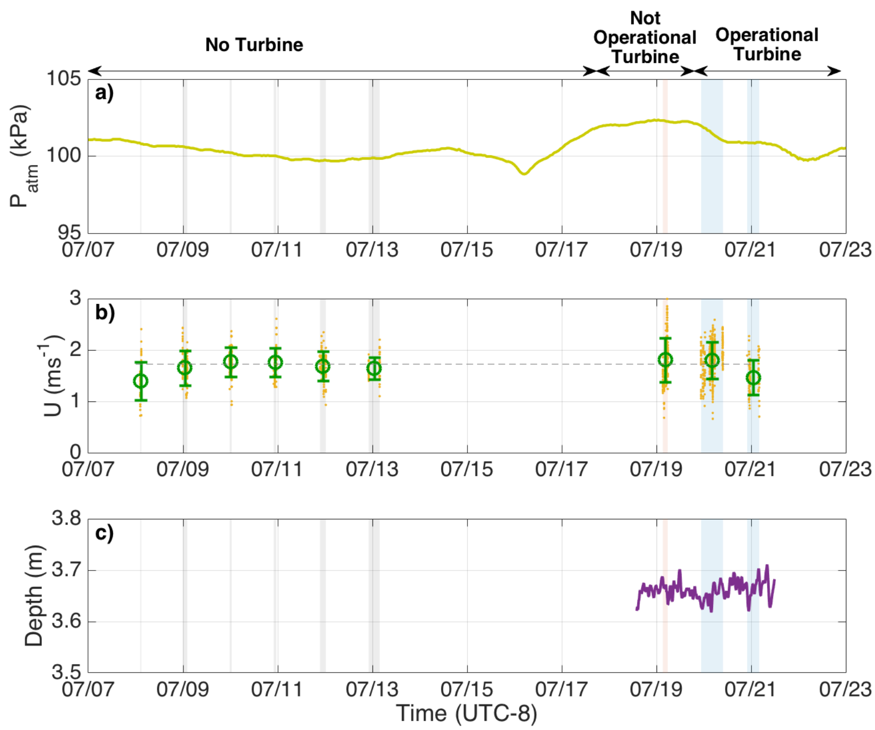

Figure A.16: a) Atmospheric pressure from Igiugig Airport weather station, b) Hub-height velocity upstream of the turbine: instantaneous velocity in orange, and daily averages in dark green, and c) water depth measurements upstream of the turbine. In all figures shaded areas correspond with the times of the three data sets from the SWIFT buoy: no turbine (gray), not operational turbine (red), and operational turbine (blue).

References

[1] G. Cada, J. Ahlgrimm, M. Bahleda, T. Bigford, S. Stavrakas, D. Hall, R. Moursund, M. Sale, Potential impacts of hydrokinetic and wave energy conversion technologies on aquatic environments, Fisheries 32 (2007) 174–181.

[2] G. Boehlert, A. Gill, Environmental and ecological effects of ocean renewable energy development: a current synthesis, Oceanography 23 (2010) 68–81.

[3] B. Polagye, B. Van Cleve, A. Copping, K. Kirkendall, Environmental Effects of Tidal Energy Development: Proceedings of a Scientific Workshop March 22-25, 2010, Technical Report, US National Oceanographic and Atmospheric Administration, 2011.

[4] M. Adaramola, P.-Å. Krogstad, Experimental investigation of wake effects on wind turbine performance, Renewable Energy 36 (2011) 2078–2086.

[5] L. Myers, S. Bahaj, An experimental investigation simulating flow effects in first generation marine current energy converter arrays, Renewable Energy 37 (2012) 28 – 36.

[6] V. S. Neary, B. Gunawan, C. Hill, L. P. Chamorro, Near and far field flow disturbances induced by model hydrokinetic turbine: ADV and ADP comparison, Renewable Energy 60 (2013) 1–6.

[7] M. De Dominicis, R. O. Murray, J. Wolf, Multi-scale ocean response

to a large tidal stream turbine array, Renewable Energy 114 (2017) 1160–1179.

[8] A. J. G. Brown, S. P. Neill, M. J. Lewis, Tidal energy extraction in three-dimensional ocean models, Renewable Energy 114 (2017) 244–257.

[9] L. Chamorro, C. Hill, S. Morton, C. Ellis, R. Arndt, F. Sotiropoulos, On the interaction between a turbulent open channel flow and an axial-flow turbine, Journal of Fluid Mechanics 716 (2013) 658–670.

[10] S. Kang, X. Yang, F. Sotiropoulos, On the onset of wake meandering for an axial flow turbine in a turbulent open channel flow, Journal of Fluid Mechanics 744 (2014) 376–403.

[11] L. Chamorro, C. Hill, V. Neary, B. Gunawan, R. Arndt, F. Sotiropoulos, Effects of energetic coherent motions on the power and wake of an axial-flow turbine, Physics of Fluids (1994-present) 27 (2015) 055104.

[12] L. Myers, A. Bahaj, Experimental analysis of the flow field around horizontal axis tidal turbines by use of scale mesh disk rotor simulators, Ocean Engineering 37 (2010) 218–227.

[13] S. Kang, I. Borazjani, J. Colby, F. Sotiropoulos, Numerical simulation of 3d flow past a real-life marine hydrokinetic turbine, Advances in Water Resources 39 (2012) 33–43.

[14] T. Blackmore, W. Batten, A. Bahaj, Influence of turbulence on the wake of a marine current turbine simulator, in: Proceedings of the

Royal Society of London A: Mathematical, Physical and Engineering Sciences, volume 470, The Royal Society, p. 20140331.

[15] M. Boudreau, G. Dumas, Comparison of the wake recovery of the axial-flow and cross-flow turbine concepts, Journal of Wind Engineering and Industrial Aerodynamics 165 (2017) 137–152.

[16] S. Chawdhary, C. Hill, X. Yang, M. Guala, D. Corren, J. Colby, F. Sotiropoulos, Wake characteristics of a triframe of axial-flow hydrokinetic turbines, Renewable Energy 109 (2017) 332–345.

[17] L. Myers, A. Bahaj, Wake studies of a 1/30th scale horizontal axis marine current turbine, Ocean Engineering 34 (2007) 758–762.

[18] L. Chamorro, D. Troolin, S. Lee, R. Arndt, F. Sotiropoulos, Three-dimensional flow visualization in the wake of a miniature axial-flow hydrokinetic turbine, Experiments in Fluids 54 (2013) 1–12.

[19] P. Bachant, M. Wosnik, Characterising the near-wake of a cross-flow turbine, Journal of Turbulence 16 (2015) 392–410.

[20] Y. Chen, B. Lin, J. Lin, S. Wang, Experimental study of wake structure behind a horizontal axis tidal stream turbine, Applied Energy 196 (2017) 82–96.

[21] A. Day, A. Babarit, A. Fontaine, Y.-P. He, M. Kraskowski, M. Murai, I. Penesis, F. Salvatore, H.-K. Shin, Hydrodynamic modelling of marine renewable energy devices: A state of the art review, Ocean Engineering 108 (2015) 46 – 69.

[22] B. Polagye, R. Cavagnaro, A. Niblick, T. Hall, J. Thomson, A. Aliseda, Cross-flow turbine performance and wake characterization, in: Proceedings of the 1st Marine Energy Technology Symposium (METS13), Washington, DC.

[23] T. Burton, D. Sharpe, N. Jenkins, E. Bossanyi, Wind energy handbook, John Wiley & Sons, 2001.

[24] W. Batten, A. Bahaj, A. Molland, J. Chaplin, The prediction of the hydrodynamic performance of marine current turbines, Renewable Energy 33 (2008) 1085–1096.

[25] D. Forbush, B. Polagye, J. Thomson, L. Kilcher, J. Donegan, J. McEntee, Performance characterization of a cross-flow hydrokinetic turbine in sheared inflow, International Journal of Marine Energy 16 (2016) 150–161.

[26] J. Thomson, Wave breaking dissipation observed with SWIFT drifters, Journal of Atmospheric and Oceanic Technology 29 (2012) 1866–1882.

[27] S. Harding, L. Kilcher, J. Thomson, Turbulence measurements from compliant moorings - part I: motion characterization, Journal of Atmospheric and Oceanic Technology (2017).

[28] L. Kilcher, S. Harding, J. Thomson, S. Nylund, Turbulence measurements from compliant moorings - part II: motion correction, Journal of Atmospheric and Oceanic Technology (2017).

[29] D. Goring, V. Nikora, Despiking acoustic doppler velocimeter data, Journal of Hydraulic Engineering 128 (2002) 117–126.

[30] M. Guerra, J. Thomson, Turbulence measurements from 5-beam acoustic doppler current profilers, Journal of Atmospheric and Oceanic Technology (2017).

[31] J. Thomson, B. Polagye, V. Durgesh, M. Richmond, Measurements of turbulence at two tidal energy sites in Puget Sound, WA, IEEE Journal of Oceanic Engineering 37 (2012) 363–374.

[32] P. J. Wiles, T. P. Rippeth, J. H. Simpson, P. J. Hendricks, A novel technique for measuring the rate of turbulent dissipation in the marine environment, Geophysical Research Letters 33 (2006).

[33] P. Rusello, E. Cowen, Turbulent dissipation estimates from pulse coherent doppler instruments, in: Proceedings. IEEE/OES 10th Current, Waves and Turbulence Measurements (CWTM), Monterey, CA., IEEE, pp. 167–172.